arXiv:2105.09239v1 [cond-mat.str-el] 19 May 2021

Origin of insulating ferromagnetism in iron oxychalcogenide $Ce_2O_2FeSe_2$

Ling-Fang Lin,[1] Yang Zhang,[1] Gonzalo Alvarez,[2] Adriana Moreo,[1,3] and Elbio Dagotto[1,3]

[1] *Department of Physics and Astronomy, University of Tennessee, Knoxville, Tennessee 37996, USA*
[2] *Computational Sciences & Engineering Division and Center for Nanophase Materials Sciences, Oak Ridge National Laboratory, Oak Ridge, TN 37831, USA*
[3] *Materials Science and Technology Division, Oak Ridge National Laboratory, Oak Ridge, Tennessee 37831, USA*

An insulating ferromagnetic (FM) phase exists in the quasi-one-dimensional iron chalcogenide $Ce_2O_2FeSe_2$ but its origin is unknown. To understand the FM mechanism, here a systematic investigation of this material is provided, analyzing the competition between ferromagnetic and antiferromagnetic tendencies and the interplay of hoppings, Coulomb interactions, Hund's coupling, and crystal-field splittings. Our intuitive analysis based on second-order perturbation theory shows that large entanglements between doubly-occupied and half-filled orbitals play a key role in stabilizing the FM order in $Ce_2O_2FeSe_2$. In addition, via many-body computational techniques applied to a multi-orbital Hubbard model, the phase diagram confirms the proposed FM mechanism, in agreement with experiments.

Introduction.- Over decades, the universal understanding of the superexchange phenomenon in transition metal compounds attracted the attention of the Condensed Matter community [1–4]. Anderson's superexchange theory based on atomic-limit second-order perturbation theory in the hopping amplitudes dominates for many insulating materials [1–3]. This case is illustrated in Fig. 1(a): the Heisenberg coupling between two half-filled orbitals should be antiferromagnetic (AFM). On the other hand, via third-order perturbation theory the case involving a half-filled orbital and empty orbital, coupled with partially filled orbitals via Hund coupling $J_{\rm H}$, Fig. 1(b), was shown to lead to ferromagnetic (FM) order. Being third order, the magnitude of the FM coupling is smaller than the AFM superexchange. Also at third-order, the case of overlap between full-filled and half-filled orbitals, also coupled with partially filled orbitals via $J_{\rm H}$, Fig. 1(c) should also be FM [2, 5].

Generally, magnetic insulating materials exhibit multiple types of active interactions, including the kinetic exchange, normally AFM and dominant; direct exchange, which is FM and weak; and *etc.* [1]. For stronger FM order, often mechanisms such as double exchange are invoked as in doped manganites, but in this case the state is metallic [6, 7]. Thus, the canonical broad stereotype is that magnetic insulators are primarily antiferromagnets and magnetic metals primarily ferromagnets.

However, insulators exhibiting robust FM states that overwhelm AFM tendencies have been observed experimentally, such as perovskite $BiMnO_3$ with orbital order [9], double perovskite Sr_3OsO_6 [10], 90° bond $CrSiTe_3$ [11] and others [12–21]. Some of these materials with simple 180° and 90° bond case could be qualitatively understood by the semiempirical Goodenough-Kanamori-Anderson (GKA) rules [1–3, 22–25]. But many other cases are more difficult. For instance, the cation-anion-cation bond angle often deviates substantially away from 180° or 90°, or the crystal-field symmetry of the magnetic ion is more complicated than the well-explored octahedral coordination. Moreover, the many FM insulators known to exist experimentally suggest that the GKA rules – based on atomic-limit third-order perturbation theory – are probably incomplete.

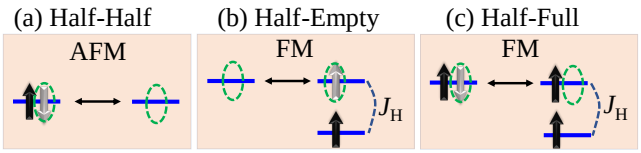

FIG. 1. Sketch of the basic superexchange cases known (a-c). Blue lines and black arrows represent the orbitals and electrons with spin up or down, respectively. The two-way thin arrows indicated the overlap between inter-site orbitals. Grey thick arrows in the green dashed circles indicate virtual hopping processes. Real materials might host more than one exchange, introducing competition between them [8].

In this publication, we propose an explanation for the origin of the FM insulating state in quasi-one-dimensional (Q1D) $Ce_2O_2FeSe_2$ (COFS) chain system. The new concept discussed here is that, due to geometrical reasons, some of the *inter-orbital* electronic hopping amplitudes can become comparable, or even larger, than the intra-orbital hoppings, allowing for FM order to dominate over AFM order. We show explicitly that for COFS, in the regime of robust Hund coupling, remarkably FM order defeats AFM order unveiling a non-canonical mechanism to generate a FM insulator. Our study only requires second-order perturbation theory and thus is directly comparable in magnitude to Anderson's simple superexchange.

Model system.- Low dimensional materials and models have recently received considerable attention [26–37]. Recent experiments showed that Q1D COFS, structurally related to the *Ln*FeAsO family of superconductors, has a large magnetic moment $\sim 3.3\ \mu_{\rm B}$ on Fe^{2+} ($3d$ $n = 6$ electrons) and is ferromagnetically coupled along the dominant chain direction [38, 39]. Each chain is made of distorted edge-sharing $FeSe_4$ tetrahedra and the Fe-Se-Fe bond is 71°, highly deviating from 90°. Experiments showed that the Fe-Se-Ce interactions are much

weaker than the Fe-Se-Fe nearest-neighbor (NN) interactions, indicating that COFS is essentialy a 1D chain system [39], with weak coupling between chains. The experimental band gap ~ 0.64 eV indicates this material is on the insulating side of the metal-Mott boundary [38]. These experimental studies suggest that 1D COFS, and its robust magnetic order setting at 176 K, is an excellent candidate to explore variations of the GKA rules to explain FM insulating states.

DFT Results.- From density functional theory (DFT) calculations [40–42], the band structure of the non-interacting non-magnetic phase of COFS is clearly more dispersive along the chain direction (Γ-X / S-Y path) than other directions, indicating dominant one-dimensional behavior along the k_x axis, as shown in Figs. 2 (a) and (b). The relevant hopping amplitudes and crystal field splitting energies for the five $3d$ iron orbitals were extracted using the maximally localized Wannier functions [43, 44]. The dominated parameters are in Fig. 2 (c). After turning on the Hubbard U and magnetism, experiments suggest that COFS will become a Mott insulator with no bands crossing the Fermi level.

As shown in Fig. 2 (c), the orbital $d_{x^2-y^2}$ has the largest NN intra-orbital hopping and the lowest onsite crystal-field energy level. Besides the intra-orbital hoppings, our results indicate that the inter-orbital hoppings – corresponding to non-zero off-diagonal matrix elements – are also robust. These important inter-orbital hoppings lead to orbital entanglement and, thus, the five orbitals can be naturally divided into three sectors: sector 1 $\{d_{z^2}\}$ (primarily isolated), 2 $\{d_{x^2-y^2}, d_{yz}\}$, and 3 $\{d_{xz}, d_{xy}\}$. From the DFT hopping amplitudes and crystal fields, the total bandwidth for each sector is roughly estimated to be $\sim$ 1, 2.3, and 1 eV, respectively, with sector 2 having the largest bandwidth compared to others.

If only the kinetic term and crystal-field splitting were included, i.e., at $U = 0$ and $J_{\rm H} = 0$, sectors 2 and 3 will form entangled bonding and antibonding states with robust band gaps between them (Fig. 2 (d) left panel). The 6 electrons would fill energy levels with 3 spin up and 3 spin down to form a non-magnetic state, with electrons distributed in each sector as {2, 2, 2}, respectively. On the other hand, at large U and $J_{\rm H}$ (Fig. 2 (d) right panel), then all orbitals are decoupled and localized to form a Mott phase, and the 6 electrons fill energy levels with 5 spins up and 1 spin down leading to a high-spin state. In this case, electrons are distributed in each sector as {1, 3, 2}, respectively. The extra electron (pointing down) transfers from sector 1 to sector 2, and finally to $d_{x^2-y^2}$, due to its lowest crystal-field energy level. Because experimentally COFS is a Mott insulator with valence Fe^{2+} and in a high-spin state [38, 39] from this analysis the most relevant three orbitals are $\{d_{z^2}, d_{yz}, d_{x^2-y^2}\}$ from sectors 1 and 2 and are, thus, chosen to be the basis in our model Hamiltonian analysis below. The three orbitals $\{d_{z^2}, d_{yz}, d_{x^2-y^2}\}$, are labeled as $\{\gamma_0, \gamma_1, \gamma_2\}$ for simplicity.

Figures 2 (e) and (f) provide an intuitive visual perspective of the effective orbitals and the overlaps between orbital γ_1 for Fe1 and γ_2 for Fe2. Clearly, the effective orbitals are a combination of the d-orbital from Fe and the p-orbital from Se. The dominant overlaps are mainly contributed by the p-orbitals on Se site, showing that Se as the Fe-Fe bridge plays an important role in the hybridization. A direct overlap between d-orbitals are also found to be present, probably due to the short distance ($\sim$ 2.84 Å) between NN irons. The entanglements between orbitals, compatible with the large value of the hopping amplitude t_{12}, plays a crucial rule on this multiorbital chain system, as discussed below.

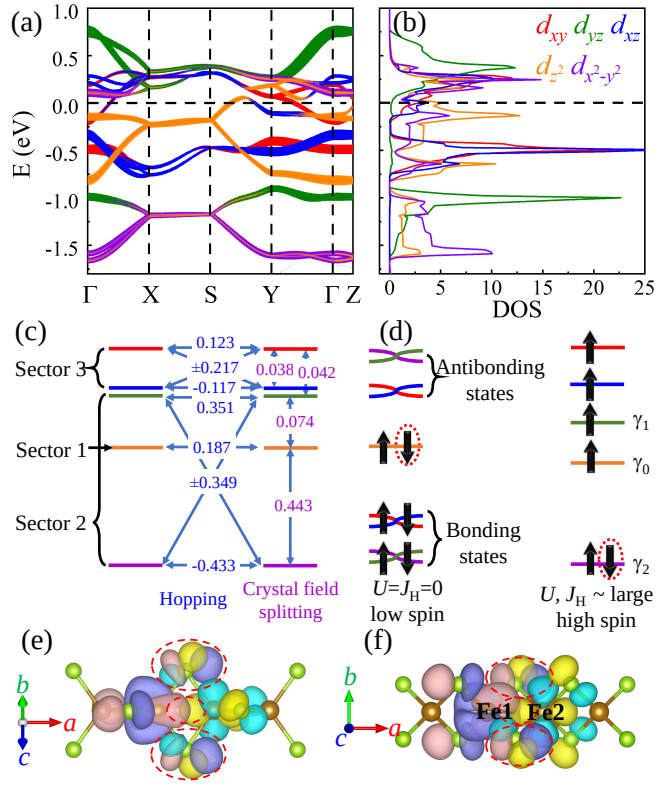

FIG. 2. (a) Iron $3d$ orbital-resolved band structure and (b) DOS, from DFT calculations for the non-magnetic phase. (c) Sketches of the crystal-field splitting and the dominant NN hopping parameters for the five orbitals. (d) Sketches of spin configurations at small U and $J_{\rm H}$ (left) and large U and $J_{\rm H}$ (right). The total population of electrons considered is 6 electrons to fill the energy levels, as shown by the thick arrows. (e)-(f) Plot of the effective Wannier functions (WF) of orbital γ_1 for Fe1 (in pink and purple) and γ_2 for Fe2 (in blue and yellow). The robust overlap between these two WFs, which is related to the amplitude of hoppings t_{12}, are indicated by the dashed red ovals.

Hubbard Model.- To better understand the magnetic properties of COFS, an effective three-orbital Hubbard model for the dominant Fe chain was constructed [45]. A tight-binding kinetic energy and on-site Coulomb interaction energy terms $H = H_k + H_{int}$ are included in the

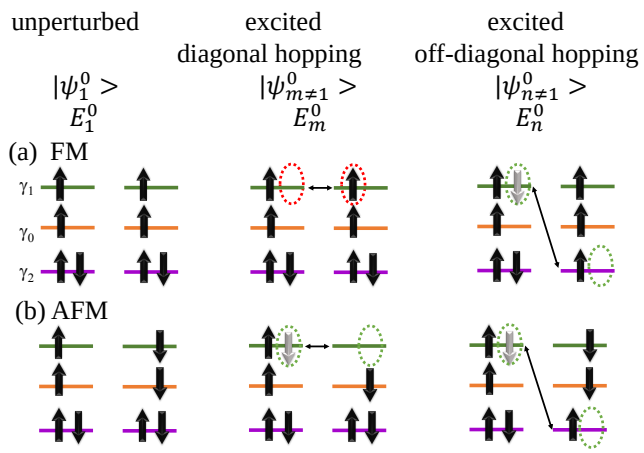

FIG. 3. Sketches of unperturbed and excited states for diagonal and off-diagonal hoppings. Both FM and AFM cases are considered. Note that for the FM case, the diagonal hopping is forbidden (red ovals) due to Pauli exclusion principle.

model. The kinetic component is

$$H_k = \sum_{i\sigma\gamma\gamma'} t_{\gamma\gamma'}(c^\dagger_{i\sigma\gamma}c_{i+1\sigma\gamma'} + H.c.) + \sum_{i\gamma\sigma}\Delta_\gamma n_{i\gamma\sigma}, \quad (1)$$

where the first term represents the hopping of an electron from orbital γ at site i to orbital γ' at the NN site $i+1$. For simplicity, only the most important NN hopping amplitudes (eV units) are included in our model [46],

$$t_{\gamma\gamma'} = \begin{bmatrix} 0.187 & -0.054 & 0.020 \\ 0.054 & 0.351 & -0.349 \\ 0.020 & 0.349 & -0.433 \end{bmatrix}. \quad (2)$$

Δ_γ is the crystal-field splitting of orbital γ, i.e. $\Delta_0 = -0.277$, $\Delta_1 = -0.203$, $\Delta_2 = -0.720$ eV, respectively. The total kinetic energy bandwidth W is 2.085 eV.

The electronic interaction portion of the Hamiltonian – including the intraorbital Hubbard repulsion, interorbital repulsion at different orbitals, Hund's coupling, and pair hopping terms – is written as:

$$H_{int} = U\sum_{i\gamma} n_{i\uparrow\gamma}n_{i\downarrow\gamma} + (U' - \frac{J_{\rm H}}{2})\sum_{\substack{i\\ \gamma<\gamma'}} n_{i\gamma}n_{i\gamma'}$$
$$-2J_{\rm H}\sum_{\substack{i\\ \gamma<\gamma'}} \mathbf{S}_{i,\gamma}\cdot\mathbf{S}_{i,\gamma'} + J_{\rm H}\sum_{\substack{i\\ \gamma<\gamma'}}(P^\dagger_{i\gamma}P_{i\gamma'} + H.c.). \quad (3)$$

where $U' = U - 2J_{\rm H}$ is used and $P_{i\gamma}{=}c_{i\downarrow\gamma}c_{i\uparrow\gamma}$.

Second-order perturbation theory.- Consider the large U limit where the hoppings $t_{\gamma\gamma'}{\ll}U, J_{\rm H}$ are the perturbation. A sketch is provided in Fig. 3, considering 2 sites and 3 orbitals with population {1, 1, 2} and focusing on the U, U', $J_{\rm H}$ and Δ_γ terms (the pair-hopping is widely considered to play a secondary role in calculations of this kind). For nondegenerate states, it is well known that the second-order perturbation theory to the ground state (state 1) always lowers the energy by:

$$\Delta E_1 = -\sum_{m\neq1}\frac{|\langle\psi_m^0|H'|\psi_1^0\rangle|^2}{E_m^0 - E_1^0}. \quad (4)$$

For both the FM and AFM unperturbed states, the ground state atomic energy is

$$E_1^0 = 2U + 10U' - 6J_{\rm H} + 2\Delta_0 + 2\Delta_1 + 4\Delta_2. \quad (5)$$

(a) For the FM case, the intra-orbital hopping is forbidden due to the Pauli principle. As for the excited state induced by the off-diagonal hopping, the energy is

$$E_{exc}^0 = 2U + 11U' - 7J_{\rm H} + 2\Delta_0 + 3\Delta_1 + 3\Delta_2. \quad (6)$$

By using this second-order perturbation theory, the DFT-deduced hoppings and crystal fields, and the widely employed ratio $J_{\rm H}/U = 1/4$ for materials of the family of iron superconductors, it can be shown that the total gain in energy of the FM configuration due to t_{12} is

$$\Delta E_{\rm FM} = \frac{|\langle\psi_{exc}^0|H'|\psi_1^0\rangle|^2}{E_1^0 - E_{exc}^0} = -\frac{|t_{12}|^2}{U - 3J_{\rm H} + \Delta_1 - \Delta_2}. \quad (7)$$

(b) For the AFM case, the energy of the diagonal intra-orbital hopping excited state is

$$E_{exc11}^0 = 3U + 10U' - 5J_{\rm H} + 2\Delta_0 + 2\Delta_1 + 4\Delta_2. \quad (8)$$

Thus, the gain in energy for the AFM configuration due to the intra-orbital hopping t_{11} (or t_{00}) is

$$\Delta E_{\rm AFM-11} = \frac{|\langle\psi_{exc}^0|H'|\psi_1^0\rangle|^2}{E_1^0 - E_{exc11}^0} = -\frac{|t_{11}|^2}{U + J_{\rm H}}. \quad (9)$$

For the same AFM case, the energy of the off-diagonal hopping t_{12} excited state is

$$E_{exc12}^0 = 2U + 11U' - 5J_{\rm H} + 2\Delta_0 + 3\Delta_1 + 3\Delta_2. \quad (10)$$

The gain in energy for the AFM configuration due to the off-diagonal hopping t_{12} is

$$\Delta E_{\rm AFM-12} = \frac{|\langle\psi_n^0|H'|\psi_1^0\rangle|^2}{E_1^0 - E_n^0} = -\frac{|t_{12}|^2}{U - J_{\rm H} + \Delta_1 - \Delta_2}. \quad (11)$$

The total energy gained in the AFM state from the t_{00}, t_{11} and t_{12} terms, using the same DFT and Hund parameters as in the FM case, is

$$\Delta E_{\rm AFM} = -\frac{|t_{00}|^2}{U + J_{\rm H}} - \frac{|t_{11}|^2}{U + J_{\rm H}} - \frac{|t_{12}|^2}{U - J_{\rm H} + \Delta_1 - \Delta_2}. \quad (12)$$

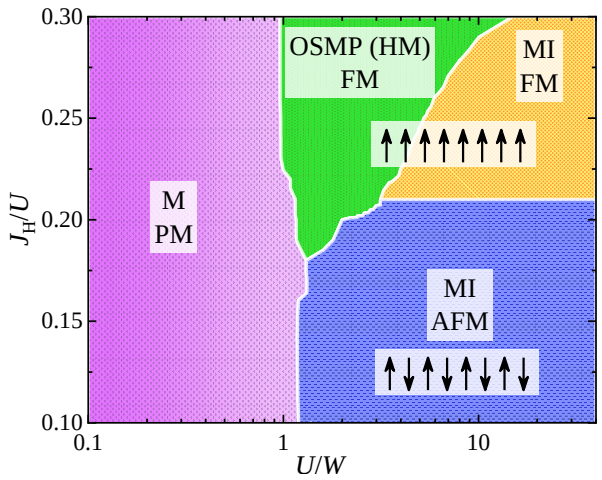

FIG. 4. DMRG phase diagram of the three-orbital Hubbard model varying U/W and J_H/U, using a $L = 16$ chain. Different phases are indicated, with the conventions metal (M), Hund metal (HM), orbital-selective Mott phase (OSMP), Mott insulator (MI), paramagnetic (PM), antiferromagnetic (AFM), and ferromagnetic (FM) phases. Some mixture and incommensurate phases exist in narrow regions near the boundaries, but are not indicated.

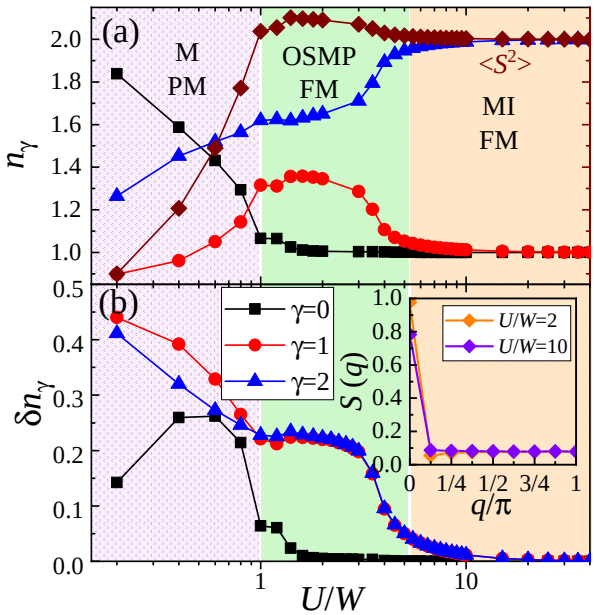

FIG. 5. (a) Orbital-resolved occupation number n_γ, mean value of the total spin squared $\langle \mathbf{S}^2 \rangle$ (in maroon color) and (b) charge fluctuations vs U/W at $J_H/U = 1/4$. Inset: spin structure factor for $U/W = 2$ and 10.

It can be shown that for $U \gtrsim 2.17$, i.e. $U/W \gtrsim 1.04$, $|\Delta E_{FM}| > |\Delta E_{AFM}|$. Then, the large off-diagonal hopping amplitude plays the key role on the dominance of the FM order over the more canonical AFM order. Note the important role of the Hund coupling. In fact, repeating the calculation for $J_H = 0$ the result is reversed and the AFM state wins. In between small and robust J_H, a transition AFM-FM occurs. Specifically, for $U = 10$ eV, the critical ratio is $J_H/U \sim 0.2$ as in the density matrix renormalization group (DMRG) results next.

DMRG & Phase diagram.- As shown in Fig. 4, the magnetic phase diagram was calculated varying U/W and J_H/U by using DMRG technique as implemented in DMRG++ software developed by one of us [47–51]. We found four dominant regimes stable in our calculations: (1) M-PM, (2) MI-AFM, (3) OSMP-FM, and (4) MI-FM. At $U/W \lesssim 1$, the system is metallic PM (M-PM) and non-magnetic, as expected. As U/W increases (in particular as $U/W \gtrsim 1$), the system becomes a Mott insulator with AFM spin ordering up-down at $J_H/U \lesssim 0.21$ (MI-AFM). Moreover, by increasing J_H/U, the system now enters a FM region. Interestingly, at intermediate U/W and $0.21 \lesssim J_H/U \lesssim 0.30$, due to the strong competition between J_H/U and U/W the system is in exotic OSMP-FM state with the selective localization of electrons on one orbital while other orbitals remain metallic with itinerant electrons. This state was extensively studied in recent literature [36, 52, 53] and will not be discussed here further. At both large U/W and J_H/U, the system develops a gap and becomes Mott insulating, defining the MI-FM state of our main focus. According to experimental results [38, 39], the undoped parent phase of COFS should be located at the MI-FM phase. In this region, the large Hubbard U renders all orbitals localized and in a high-spin state leading to a Mott phase, in the unusual FM configuration explained in the previous section via second-order perturbation theory.

For the prototypical value $J_H/U = 1/4$, the electronic occupancy and local moment are shown in Fig. 5 (a). In the small-U metallic PM phase, the n_γ values of all three orbitals evolve smoothly from the noninteracting limit with increasing U. This process can be described as the extra electron gradually transferring from sector 1 to sector 2 until the critical $U \sim W$. When $U/W \gtrsim 4$ and arriving to the MI-FM phase, the extra electron has totally transferred to γ_2, leading to $n_2 = 2$, while $n_0 = n_1 = 1$. The spin-moment local moment as presented in Fig. 5 (a) saturates to value 2 in the MI-FM region and the fluctuations of all three orbitals are suppressed.

The structure factors $S(q)$ for $U/W = 2$ and 10 are shown in the inset of Fig. 5 (b). Clearly, $S(q)$ displays a sharp peak at $q = 0$ for both $U/W = 2$ and 10, indicating that FM spin states can be robust within the OSMP and MI regions. The FM spin state within the MI region is also in good agreement with experiments [38, 39]. The corresponding single-particle spectra and DOS for $J_H/U = 1/4$ and $U/W = 10$ are in the SM [46]. Orbitals γ_0 and γ_1 are half-filled with a large Mott gap, while orbital γ_2 is full-filled, then the final gap becomes ~ 2.5 eV.

Conclusions. - The iron chalcogenide COFS with $n = 6$ electrons per Fe ion was studied by DFT, by DMRG applied to a three-orbital Hubbard model, and

by second-order perturbation theory to gain insight into the intuitive physics of our results. Our investigations show that in COFS inter-orbital electronic hopping amplitudes can become comparable or larger than the intra-orbital hoppings due to geometrical reasons. The resulting large inter-orbital hoppings play a key role in stabilizing an insulating ferromagnetic state. The proposed FM mechanism was confirmed computationally via DMRG. The rich phase diagram unveiled here suggests that COFS is located at strong U/W and at the realistic value $J_{\rm H}/U = 1/4$, in agreement with experimental results [38, 39]. The proposed mechanism requires $J_{\rm H}$ to be robust, as in the family of iron supercondcutors. We predict that the similar chain system Na_2FeX_2 [54] should also exhibit FM coupling along the chain direction.

Acknowledgments. - The work of L.-F.L., Y.Z., A.M. and E.D. was supported by the U.S. Department of Energy (DOE), Office of Science, Basic Energy Sciences (BES), Materials Sciences and Engineering Division. G.A. was partially supported by the scientific Discovery through Advanced Computing (SciDAC) program funded by U.S. DOE, Office of Science, Advanced Scientific Computing Research and BES, Division of Materials Sciences and Engineering. All the calculations were carried out at the University of Tennessee Advanced Computational Facility (ACF).

[1] P. W. Anderson, Phys. Rev. **115**, 2 (1959).
[2] J. B. Goodenough, Magnetism and the Chemical Bond, Vol. 1 (Interscience publishers (Wiley), New York, 1963).
[3] P. W. Anderson, in Solid state physics, Vol. 14 (Elsevier, 1963) pp. 99–214.
[4] L.-F. Lin, N. Kaushal, C. Sen, A. D. Christianson, A. Moreo, and E. Dagotto, Phys. Rev. B **103**, 184414 (2021).
[5] H. Weihe and H. U. Güdel, Inorg. Chem. **36**, 3632 (1997).
[6] E. Dagotto, T. Hotta, and A. Moreo, Phys. Rep. **344**, 1 (2001).
[7] M. Mayr, A. Moreo, J. A. Vergés, J. Arispe, A. Feiguin, and E. Dagotto, Phys. Rev. Lett. **86**, 135 (2001).
[8] The present study suggests that COFS host the competition between mechanism (a) and (c). Interestingly, the abnormally large *inter-orbital hopping* amplitude together with large $J_{\rm H}$ allows the FM kinetic mechanism (c) to dominate over (a).
[9] A. Moreira dos Santos, A. K. Cheetham, T. Atou, Y. Syono, Y. Yamaguchi, K. Ohoyama, H. Chiba, and C. N. R. Rao, Phys. Rev. B **66**, 064425 (2002).
[10] Y. K. Wakabayashi, Y. Krockenberger, N. Tsujimoto, T. Boykin, S. Tsuneyuki, Y. Taniyasu, and H. Yamamoto, Nat. Commun. **10**, 1 (2019).
[11] J. Zhang, X. Cai, W. Xia, A. Liang, J. Huang, C. Wang, L. Yang, H. Yuan, Y. Chen, S. Zhang, et al., Phys. Rev. Lett. **123**, 047203 (2019).
[12] J. Q. Yan, J. S. Zhou, and J. B. Goodenough, Phys. Rev. B **70**, 014402 (2004).
[13] V. V. Mehta, N. Biskup, C. Jenkins, E. Arenholz, M. Varela, and Y. Suzuki, Phys. Rev. B **91**, 144418 (2015).
[14] Q. Zhang, A. Gao, F. Meng, Q. Jin, S. Lin, X. Wang, D. Xiao, C. Wang, K.-j. Jin, D. Su, et al., Nat. Commun. **12**, 1 (2021).
[15] A. A. Taskin, A. N. Lavrov, and Y. Ando, Phys. Rev. Lett. **90**, 227201 (2003).
[16] H. Das, U. V. Waghmare, T. Saha-Dasgupta, and D. D. Sarma, Phys. Rev. Lett. **100**, 186402 (2008).
[17] H. L. Feng, Z. Deng, C. U. Segre, M. Croft, S. H. Lapidus, C. E. Frank, Y. Shi, C. Jin, D. Walker, and M. Greenblatt, Inorg. Chem. (2020).
[18] M. A. McGuire, H. Dixit, V. R. Cooper, and B. C. Sales, Chem. Mater. **27**, 612 (2015).
[19] C. Gong, L. Li, Z. Li, H. Ji, A. Stern, Y. Xia, T. Cao, W. Bao, C. Wang, Y. Wang, et al., Nature (London) **546**, 265 (2017).
[20] Z. Huang, D. Liu, A. Mansikkamäki, V. Vieru, N. Iwahara, and L. F. Chibotaru, Phys. Rev. Research **2**, 033430 (2020).
[21] M. Steiner, J. Villain, and C. Windsor, Adv. Phys. **25**, 87 (1976).
[22] P. W. Anderson, Phys. Rev. **79**, 350 (1950).
[23] J. B. Goodenough, Phys. Rev. **100**, 564 (1955).
[24] J. B. Goodenough, J. Phys. Chem. Solids **6**, 287 (1958).
[25] J. Kanamori, J. Phys. Chem. Solids **10**, 87 (1959).
[26] K. Kuroki, S. Onari, R. Arita, H. Usui, Y. Tanaka, H. Kontani, and H. Aoki, Phys. Rev. Lett. **101**, 087004 (2008).
[27] B. Pandey, Y. Zhang, N. Kaushal, R. Soni, L.-F. Lin, W.-J. Hu, G. Alvarez, and E. Dagotto, Phys. Rev. B **103**, 045115 (2021).
[28] L.-F. Lin, N. Kaushal, Y. Zhang, A. Moreo, and E. Dagotto, Phys. Rev. Mater. **5**, 025001 (2021).
[29] L.-F. Lin, Y. Zhang, A. Moreo, E. Dagotto, and S. Dong, Phys. Rev. Lett. **123**, 067601 (2019).
[30] Y. Zhang, L.-F. Lin, A. Moreo, G. Alvarez, and E. Dagotto, Phys. Rev. B **103**, L121114 (2021).
[31] Y. Zhang, L.-F. Lin, A. Moreo, S. Dong, and E. Dagotto, Phys. Rev. B **100**, 184419 (2019).
[32] Y. Zhang, L.-F. Lin, A. Moreo, S. Dong, and E. Dagotto, Phys. Rev. B **101**, 144417 (2020).
[33] Y. Zhang, L.-F. Lin, A. Moreo, S. Dong, and E. Dagotto, Phys. Rev. B **101**, 174106 (2020).
[34] J. Herbrych, J. Heverhagen, G. Alvarez, M. Daghofer, A. Moreo, and E. Dagotto, Proc. Natl. Acad. Sci. USA **117**, 16226 (2020).
[35] B. Pandey, L.-F. Lin, R. Soni, N. Kaushal, J. Herbrych, G. Alvarez, and E. Dagotto, Phys. Rev. B **102**, 035149 (2020).
[36] N. Patel, A. Nocera, G. Alvarez, A. Moreo, S. Johnston, and E. Dagotto, Comm. Phys. **2**, 64 (2019).
[37] J. Herbrych, J. Heverhagen, N. D. Patel, G. Alvarez, M. Daghofer, A. Moreo, and E. Dagotto, Phys. Rev. Lett. **123**, 027203 (2019).
[38] E. E. McCabe, D. G. Free, and J. S. Evans, Chem. Comm. **47**, 1261 (2011).
[39] E. E. McCabe, C. Stock, J. L. Bettis, M. H. Whangbo, and J. S. O. Evans, Phys. Rev. B **90**, 235115 (2014).
[40] G. Kresse and D. Joubert, Phys. Rev. B **59**, 1758 (1999).

[41] P. E. Blöchl, Phys. Rev. B **50**, 17953 (1994).
[42] J. P. Perdew, A. Ruzsinszky, G. I. Csonka, O. A. Vydrov, G. E. Scuseria, L. A. Constantin, X. Zhou, and K. Burke, Phys. Rev. Lett. **100**, 136406 (2008).
[43] N. Marzari and D. Vanderbilt, Phys. Rev. B **56**, 12847 (1997).
[44] A. A. Mostofi, J. R. Yates, Y.-S. Lee, I. Souza, D. Vanderbilt, and N. Marzari, Comput. Phys. Commun. **178**, 685 (2008).
[45] Hubbard-like model commonly discards the FM direct exchange as mentioned by Wei *et. al.* [55], but direct exchange could be legitimately omitted in our case since the kinetic exchange dominates over the direct exchange.
[46] See Supplemental Material for more details of the method, hopping matrix, and spectrum & DOS plot.
[47] S. R. White, Phys. Rev. Lett. **69**, 2863 (1992).
[48] S. R. White, Phys. Rev. B **48**, 10345 (1993).
[49] U. Schollwöck, Rev. Mod. Phys. **77**, 259 (2005).
[50] K. A. Hallberg, Adv. Phys. **55**, 477 (2006).
[51] G. Alvarez, Comput. Phys. Commun. **180**, 1572 (2009).
[52] R. Yu, H. Hu, E. M. Nica, J.-X. Zhu, and Q. Si, Front. Phys. **9**, 578347 (2021).
[53] J. Rincón, A. Moreo, G. Alvarez, and E. Dagotto, Phys. Rev. Lett. **112**, 106405 (2014).
[54] P. Stüble, S. Peschke, D. Johrendt, and C. Röhr, J. Solid State Chem. **258**, 416 (2018).
[55] W. Ku, H. Rosner, W. E. Pickett, and R. T. Scalettar, Phys. Rev. Lett. **89**, 167204 (2002).